Quantum Electronics **46** (1) 81–87 (2016)

EUV LITHOGRAPHY SOURCES

DOI: 10.1070/QE2016v046n01ABEH015657

High-brightness laser-induced EUV source based on tin plasma with an unlimited lifetime of electrodes

A.Yu. Vinokhodov, V.M. Krivtsun, A.A. Lash, V.M. Borisov, O.F. Yakushev, K.N. Koshelev

Abstract. **Characteristics of a source of laser-induced radiation in the extreme ultraviolet (EUV) range, obtained in a discharge between two jets of liquid tin, are investigated. The possibility of designing a high-brightness EUV source on this basis for employing in mask inspection techniques in projection EUV lithography is demonstrated. The average efficiency of converting the electric energy to radiation in the spectral range of 13.5±0.135 nm is approximately 2%/2π sr with the size of emitting plasma 0.2±0.35 mm. The possibility of producing a EUV source with a brightness of about 200 W (mm^2 sr)$^{-1}$ is demonstrated.**

Keywords: *EUV-range radiation source, EUV lithography, plasma, discharge, liquid tin jet, source radiance.*

1. Introduction

The main trend in the production of commercial semiconductors is a consistent reduction of the characteristic size of integrated circuit elements and, hence, an increase in the density of transistors on an integrated circuit (IC). Mass production of ICs utilises the method of optical projection lithography. For the foreseeable future this method has no alternative because other methods of lithographic processes (X-ray lithography, electron-beam and ion-beam lithography) though possessing a high resolution cannot provide a sufficient efficiency in mass integrated circuit production. Presently, optical lithography, which employs an excimer ArF laser ($\lambda = 193$ nm) as a radiation source, has reaches the limiting optical resolution $R = k_1\lambda/\mathrm{NA}$, where k_1 is the photolithography coefficient dependent on an employed photoresist and technological process, and NA is the numerical aperture of the lithograph objective. Even the employment of immersion lithography technologies and double exposure cannot provide obtaining the structure resolution of less than 22 nm. It has been found [1,2] that further improvement of projection lithography for mass IC production is associated with the employment of EUV sources at $\lambda \leqslant 13.5$ nm, in particular, plasma sources based both on electro-discharge plasma (DPP-sources) [3,4] and laser plasma (LPP-sources) [3,5]. A working substance in all kinds of plasma EUV sources may be Xe, Sn and eutectic alloys based on Sn and Li. Lithographs employing plasma EUV sources of both types have been already created and operate in a test regime. While in mass production LPP-sources are preferable, DPP-sources are also used in EUV lithography. In particular, measurement facilities are developed on this basis for mask inspection; they are used for testing and controlling elements of optical systems: mirrors, photoresistors.

The general tendency in EUV lithography consists in a transfer from inspection of produced integrated circuits and their following discarding to mask inspection [6]. Mask defects concerning both its multilayer coating and the topological image deposited onto it are caused by nanoparticles of size 10–50 nm settling in the process of mask fabrication, which distort the reflecting structure deposited and lead to the emergence of print defects in integrated circuits. This makes the photoresist, which has passed the whole technological cycle, unsuitable for further employment. Very strict conditions are placed on mask imperfection: at most one defect of nano-size scale per several hundred square centimetres. The cost of masks increases with optical resolution and presently amounts to almost 50% of a price of a fabricated photoresist [7]. Production of a single integrated circuit requires a set of 20–60 masks. A single error in producing a mask may cost several million dollars. Yet a diagnostic complex for mask inspection will cost about 5 million dollars, i.e., revealing just several defect masks may compensate for the cost of a diagnostic complex for mask inspection. The cost of producing a single mask for EUV lithography is 100–300 thousand dollars. In 2020, the market of such masks, according to minimal estimates, may reach 500 billion dollars. Thus, available instruments for mask inspection are the key factor of success in the EUV lithography technology.

The main element in a complex for mask inspection is a source of high-brightness EUV radiation at a wavelength of 13.5 nm. Various technologies of mask inspection necessitate light sources with a brightness in the range from 50 to approximately 1000 W (mm^2 sr)$^{-1}$, emitting in the wavelength range $\lambda = 13.5\pm0.135$ nm with the etendue of a collecting optical system of about 10^{-3}–10^{-4} mm^2 sr (etendue is determined as the product of the area of the source and the solid angle that the system's entrance pupil subtends as seen from the source). Presently, the best results in producing a high-brightness EUV source for mask inspection are demonstrated by Adlyte Ltd [8]

A.Yu. Vinokhodov, A.A. Lash 'EUV Labs' Ltd., Sirenevyi blvd. 1, Troitsk, 142190 Moscow, Russia; e-mail: avinokhod@gmail.com, lashrnd@gmail.com;
V.M. Krivtsun, K.N. Koshelev 'EUV Labs' Ltd., Sirenevyi blvd. 1, Troitsk, 142190 Moscow, Russia; Institute of Spectroscopy, Russian Academy of Sciences, ul. Fizicheskaya 5, Troitsk, 142190 Moscow, Russia;
V.M. Borisov State Research Center of the Russian Federation 'Troitsk Institute for Innovation and Fusion Research', ul. Pushkovykh 1, Troitsk, 142190 Moscow, Russia;
O.F. Yakushev 'EUV Labs' Ltd., Sirenevyi blvd. 1, Troitsk, 142190 Moscow, Russia; P.N. Lebedev Physics Institute, Russian Academy of Sciences, Leninsky prosp. 53, 119991 Moscow, Russia

Received 19 August 2014
Kvantovaya Elektronika **46** (1) 81–87 (2016)
Translated by N.A. Raspopov

which employs the LPP-method for obtaining EUV radiation. In the source, tin drops with a diameter of 60 μm were used as a target; the frequency of drop generation was 6 kHz. The average brightness of an EUV source was 350 W $(mm^2\ sr)^{-1}$. However, the obtained stability of EUV radiation from pulse to pulse (with a relative deviation $\sigma = 3\%$) was noticeably worse than required. We should also mention a high-brightness EUV source produced by Ushio Inc., which is based on laser-induced discharge tin plasma [9]. The average brightness of the source was 180 W $(mm^2\ sr)^{-1}$ at a repetition rate of discharge pulses of 10 kHz; however, the energy stability from pulse to pulse was only 6.6%. Other substantial disadvantages of this kind of sources are electrode erosion, which limits the operation life, and a substantial level of corpuscle products in plasma-chemical reactions. The source of Energetiq [10] is based on electrodeless discharge plasma in xenon. Its drawback is a very low [less than 10 W $(mm^2\ sr)^{-1}$] brightness and poor spatial stability of emitting plasma; the advantage is a low level of products in plasma-chemical reactions. Hence, up to now the problem of creating a high-brightness EUV source at a wavelength of 13.5 nm for mask inspection in lithography has not been solved yet.

In addition to brightness, stability and small size of emitting plasma, one of the principal requirements to such sources is a long service life. The most vulnerable element in the EUV sources based on laser plasma, which limits their service life, is a nozzle unit, which forms drops of a working substance. In the electro-discharge sources, such elements are electrodes, which have a service life limited by erosion to approximately 10^8 discharge pulses. Hence, the development of an LPP EUV source with the electrodes possessing an actually unlimited service life is undoubtedly of scientific and practical interest. In the present work, the electrodes of a discharge system are jets of liquid tin, which circulate in a closed loop with a pump. A similar method for organising the discharge was used in our earlier work [11], where the working substance was the Ga–Sn eutectic alloy with the atomic tin contents of 8.5% and melting temperature of 20.5 °C, which provided operation at room temperature. In such a construction of the electrode system, the working surface of electrodes (the site where the initiating laser radiation is focused and, hence, the discharge occurs) continuously regenerates, solving in this way the problem of electrode erosion. The maximal efficiency of converting electrical energy to radiation (CE) in the range $\lambda = 13.5 \pm 0.135$ nm was $1.3\%/2\pi$ sr. However, the employment of the alloy comprising Ga as a working substance resulted in considerable technological difficulties related, first of all, to the aggressive character of Ga, which prevented us from using such an EUV source in EUV lithography technologies. In the present work, we continue investigations of laser-induced DPP EUV source with jet liquid-metal electrodes; however, as a working substance, instead of the Ga–Sn eutectic alloy we have used 100% Sn. First, the employment of Sn has increased the CE; second, corpuscular products of plasma-chemical reactions with tin plasma are not as aggressive as with gallium plasma and there is a technology for neutralising the products. Hence, such a source can be used in EUV lithography technologies, in particular, in complexes for mask inspection.

2. Experimental setup

The main feature of this EUV source, which mainly determines its constructive solutions and distinguishes it from the source in [11], is that the temperature of the working substance (tin), continuously circulating around a closed loop, should be maintained in the range 260–300 °C. Figures 1 and 2 present a functional scheme and the photograph of the source taken from the side of the front flange with diagnostic sockets arranged on it. The source was a multicomponent physical installation comprised of several systems: system for pumping liquid tin with a specially designed pump, system for heating the circuit of liquid tin with the pump, system of electric power supply and discharge initiation, gas-vacuum system, and system of cooling and diagnosing the EUV radiation.

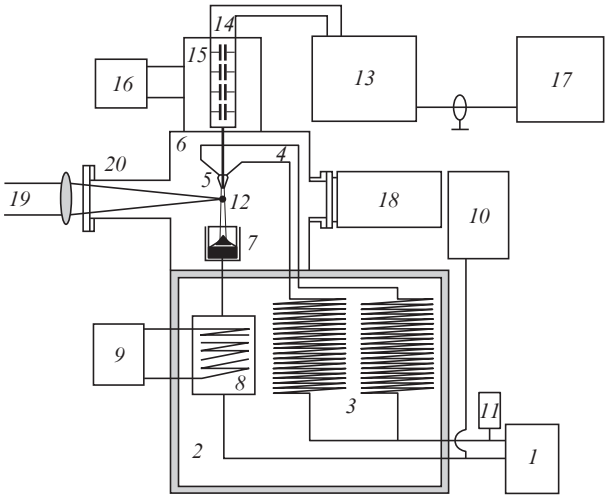

Figure 1. Functional diagram of the EUV source:
(*1*) centrifugal pump; (*2*) thermostat; (*3*) locking chokes; (*4*) supply pipes; (*5*) nozzles; (*6*) vacuum chamber; (*7*) tin collector; (*8*) oil heat exchanger; (*9*, *16*) water heat exchangers; (*10*) overhead tank; (*11*) pressure sensor; (*12*) tin jets; (*13*) pulsed discharge pump system; (*14*) discharge capacitor; (*15*) oil tank; (*17*) high-voltage rectifier; (*18*) turbo-molecular pump; (*19*) laser beam; (*20*) unit for laser radiation input.

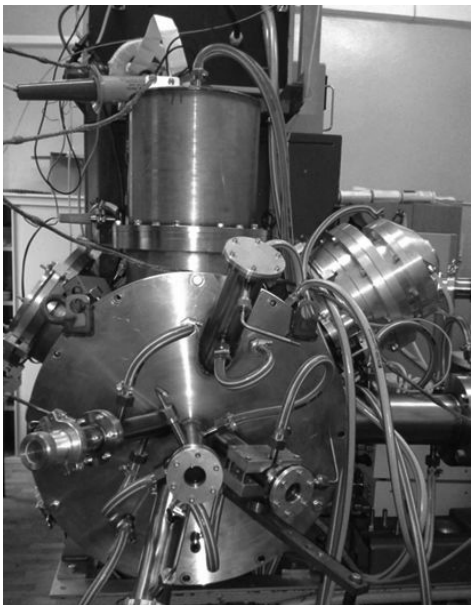

Figure 2. Photograph of the EUV source from the side of the diagnostic flange of the vacuum chamber.

The system for pumping liquid tin comprises: a centrifugal pump (*1*), a thermostat (*2*), a blocking inductor (*3*), supply tubes (*4*), nozzles (*5*) arranged in a vacuum chamber (*6*), a tin collector (*7*) with a jet splitter inside it, an oil heat exchanger (*8*) connected with a water heat exchanger (*9*), a pressure tank (*10*) and a pressure sensor (*11*). The system utilises a single loop of tin pumping, which includes both high-voltage and grounded units. Electric insulation between them was realised by using pulsed charging, blocking inductors (*3*) with the inductance $L \cong 100$ μH, and jet splitters in the tin collector. Because of the strong splashing, later this construction was replaced by the construction with a long ceramic collector, which allowed tin jets to fragment before reaching the collector. Most system elements were arranged in a thermostat, in which the temperature of 260–300 °C was maintained. Tin was pumped through the loop by a specially designed centrifugal pump with a magnetic clutch and ceramic plain bearings [12]. A vacuum gap with a pressure of about 10^{-2} mbar was used as a thermal barrier between the clutch magnets and melted tin. Figure 3 shows the dependence of the tin jet velocity [(*12*), Fig. 1] on the angular velocity of the pumping electric motor in the case of using a turbine 60 mm in diameter. One can see that the maximal attained velocity of two tin jets, with a diameter of 2 mm each, was 9 m s^{-1} at the turbine angular velocity of 53 revolutions per second. The service life of the pump tested with melted tin was several hundred hours. Note that presently we have developed and tested the pump for fusible metals and high-temperature (up to 400 °C) aggressive media, capable of providing the output pressure of up to 8 atm and jet velocities of up to 15 m s^{-1}. We plan to employ this pump in experiments with high-brightness EUV LPP-sources for producing a jet of melted metal used as a target for focused laser radiation. In experiments with a laser-induced source, we used nozzles with various cross sections: round with diameters of 2 and 3 mm, rectangular with sizes of 2.5×1 and 10×0.3 mm, and their combinations.

In the EUV source we used a pulsed system of discharge pumping [(*13*), Fig. 1], which operated on double recharging of capacitors. A low-inductance set of capacitors (*14*) comprised of ceramic capacitors (Murata) was placed in a tank (*15*), through which oil was pumped to cool them. The pump directed the oil to a water heat exchanger (*16*). The scheme of discharge initiation was triggered by IGBT modules. The main parameters of the initiation scheme (the capacitor $C = 0.67$ μF, the charge voltage $U_{dis} = 4$ kV, the time of charging the discharge capacitor $\Delta\tau = 4$ μs and the inductance of the discharge circuit $L = 12.5$ nH) provided the amplitude of the discharge current I_{dis} of up to 26 kA. The maximal rate of discharge initiation pulses f_{max} in these experiments was 4 kHz and was limited by the power of a high-voltage rectifier (*17*), although the pulsed part of the initiation scheme was capable of long-term operation at $f = 8$ kHz. However, already at $f = 4$ kHz the charging voltage reduced due to a limited power of the employed high-voltage rectifier and the energy deposited to the discharge in this case was 3.4 J, whereas at $f < 1$ kHz it was $E = 4.8$ J.

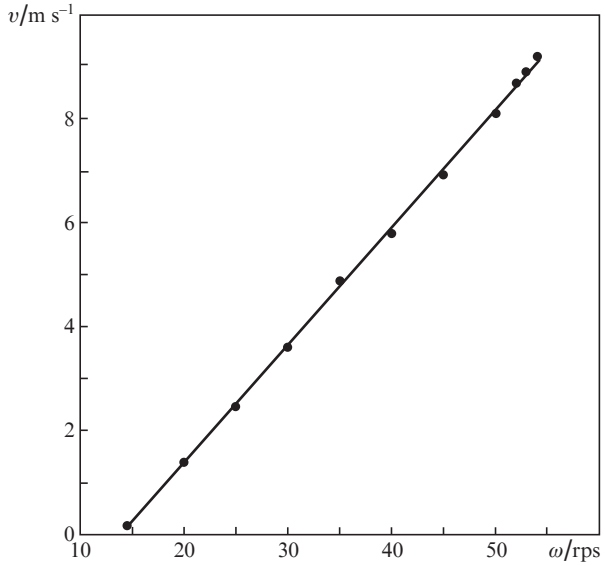

Figure 3. Velocities of two tin jets with the diameter of 2 mm vs. the rotational velocity of the pump electric motor (with the turbine diameter of 60 mm).

The case of the vacuum chamber (*6*) and all diagnostic sockets had double walls between which water was pumped. This provided efficient heat removal and long-term operation at high pulse repetition rates running no risk of overheating and nonhermeticity of the vacuum chamber, which was evacuated by a turbomolecular pump (*18*) to a pressure of 10^{-5} mbar.

Various types of heaters were used for heating all elements of the liquid tin pumping system: a quartz heater, strip heater, clamp heater and heating cable in a stainless envelope (the latter is used in a vacuum chamber). An oil circuit breaker switched off the heaters arranged in the high-voltage part of the system at the instant when a high-voltage was applied. The heaters were powered from regulated power supplies, which provided a stable temperature of all elements of the tin pumping system. The temperature was controlled by using thermocouples and PID-controllers. Altogether 16 channels were used for controlling the temperature of all elements of the tin pumping system.

A laser radiation beam (*19*) passes to the vacuum chamber through an input unit (*20*), which comprises the device for protecting the input window against argon flow contaminations. The discharge was initiated by two different Nd:YAG lasers. The first laser had the energy of $E_{las} = 80$ mJ (on a target), the FWHM pulse duration was $\tau_{FWHM} = 25$ ns, the density of radiation power was $P = 1.6\times10^9$ W cm^{-2} (with a focusing lens $F = 62$ cm) and $f_{max} = 100$ Hz. The second laser parameters were: $E_{las} = 25$ mJ (on a target), $\tau_{FWHM} = 90$ ns, $P = 10^8$ W cm^{-2} (with a focusing lens $F = 62$ cm) and $f_{max} =$ 10 kHz. By using a lens with a focal distance $F = 31$ cm we succeeded in increasing the power density of the second laser to 2.3×10^8 W cm^{-2}. Hence, the power densities of focused radiation of these lasers differed by a factor of 16. The laser radiation passed through a telescope, which provided a parallel laser beam 40 mm in diameter, then through two dielectric mirrors, a focusing lens, and was focused through the input unit of the vacuum chamber onto the grounded tin jet that was a cathode of the discharge system.

The cooling system of the source comprises water cooling of the case of the vacuum chamber, of IGBT unit in the pulsed charging scheme, of oil heat exchangers, and oil cooling of the discharge capacitors, of the pump and heat exchanger of tin pumping system. The water cooling system operated on running tap water, the oil cooling system was realised in closed loops with centrifugal pumps.

Diagnostics of EUV radiation included measurements of spectral, temporal, energy and spatial characteristics of the

source, which were performed through the sockets arranged on the input flange of the vacuum chamber (Fig. 2). The energy and shape of pulses were measured by using an AXUV-100 calibrated (absolutely) 'slow' photodiode (the capacitance was C = 10 nF) with a Mo/Si filter deposited onto its working surface and an AXUV-HS5 'fast' photodiode (C = 0.04 nF). An additional spectral filtration in the channel was made by using a multilayer Mo/Si mirror. The transmission spectral band of the channel was $\Delta\lambda$ = 12.7–13.2 nm. In addition, the energy of EUV radiation pulses was measured according to another method: by the known calibrating coefficient of the AXUV-100 photodiode without the deposited filter, which was equal to 0.19 K J^{-1}. The pulse energy was measured over the whole EUV range, and spectral dependences of filter transmission and mirror reflection were taken into account. Then, the energy of the EUV signal in the range λ = 13.5±0.135 nm was calculated. The size of the plasma domain emitting in the EUV range was measured by using a CS-8300 CCD-camera (TELI) with a phosphor screen and a pinhole camera (∅100 μm) through a zirconium filter with the transmission spectral band $\Delta\lambda$ = 5–21 nm. The spectrum of plasma emission was measured by a grazing incidence spectrometer (the spectral range is $\Delta\lambda$ = 3–61 nm, resolution is $\lambda/\delta\lambda$ = 300) with a diffraction grating 600 lines mm^{-1} and slit 40 μm. Diagnosis of the jet surface state was performed by taking photos with a short-duration photoflash. The photoflash light sources were a lamp with the duration of 10 μs or pulses of the second harmonic of the Nd:YAG laser (λ = 532 nm) with a duration of 30 ns.

3. Results

3.1. Influence of the power density of laser radiation on EUV radiation parameters

In tin plasma, efficient generation of radiation in the range around 13.5 nm occurs on the transitions of ions Sn^{+10}–Sn^{+12} at the following plasma parameters: the electron temperature is about 50 eV, the electron concentration is approximately 10^{19} cm^{-3} and the average ion charge is about 10. One of the methods for obtaining plasma with such parameters is vacuum discharge pinching in tin laser plasma that is preliminarily produced with required parameters (density, temperature, directional characteristic of plasma spread) by the radiation of the initiating laser. Figure 4 presents oscillograms of the voltage across the discharge capacitor, the pulse of EUV radiation measured by the 'slow' photodiode, the time derivative of the discharge current and the pulse of the initiating laser. In Fig. 5 one can see oscillograms of the voltage across the discharge capacitor and the pulse of EUV radiation detected by the 'fast' photodiode. The area under the oscillogram of the EUV radiation pulse detected by the 'slow' photodiode can be used for calculating the energy of the EUV radiation pulse, whereas the signal from the 'fast' photodiode records the shape of this pulse. From Fig. 4, one can see that the electric breakdown of the electrode gap occurs in approximately 200 ns after the maximum of the laser initiating pulse is reached, which corresponds to a velocity of hydrodynamic spread of laser plasma of about 10^6 cm s^{-1}. In a time lapse of 150 ns after the gap breakdown, at the current maximum, the discharge pinches, which is confirmed by a peculiarity on the oscillogram [see curve (*3*) in Fig. 4], and the pulse of EUV radiation is generated with the FWHM duration of less than 100 ns [see curve (*2*) in Fig. 5].

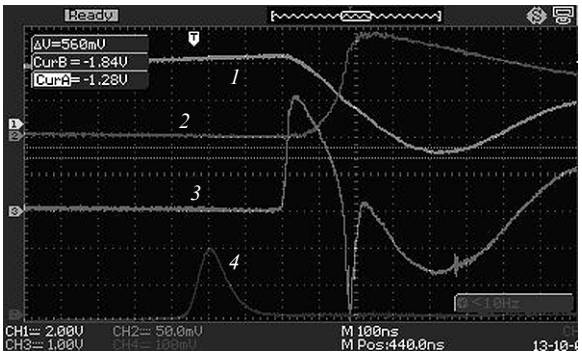

Figure 4. Oscillograms of a voltage across the discharge capacitor (*1*); of a EUV radiation pulse (*2*) detected by the 'slow' photodiode; of a derivative of the discharge current (*3*); of an initiating laser pulse (*4*).

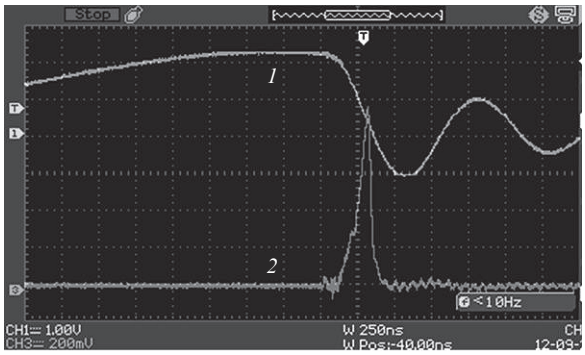

Figure 5. Oscillograms of a voltage across the discharge capacitor (*1*) and of a EUV radiation pulse (*2*) detected by the 'fast' photodiode.

Experiments on measuring the radiation energy in a wavelength range λ = 13.5±0.135 nm and size of plasma emitting in the EUV range show that results substantially differ if initiating Nd:YAG lasers with different densities of the radiation power are used. At f = 1 kHz and the laser power density P = 10^8 W cm^{-2}, the average value of CE was no greater than 1%/2π sr, and at $P = 2.3\times10^8$ W cm^{-2} it was at most 1.3%/2π sr. At the same time the employment of the laser with P = 1.6×10^9 W cm^{-2} yielded CE ≅ 2%/2π sr. In addition, the sizes of the emitting plasma substantially differ if these lasers are used. The images of plasma shown in Figs 6a and 6b correspond to the cases when the laser power densities are P = 1.6×10^9 and 10^8 W cm^{-2}, respectively. One can see that at $P = 1.6\times10^9$ W cm^{-2} the size of emitting plasma at half intensity is 0.2±0.35 mm and only concentrated near the cathode, whereas at P = 10^8 W cm^{-2} the image of plasma is mainly distributed in the gap between electrodes and has the dimensions increased to 0.7×0.7 mm. In addition, an analysis of images indicates that in the case of Fig. 6a, the plasma domain of volume 1 mm^3 emits 95% of the whole EUV energy emitted, i.e., actually all the EUV energy is emitted from the pinch domain (in the case of Fig. 6b, the corresponding value is only 35%). In Fig. 6c one can see the sum of images for 20 pulses at f = 1 kHz and $P = 10^8$ W cm^{-2}. The spatial instability of the position of emitting plasma from pulse to pulse results in that its total size near the cathode broadens to approximately 2 mm. Since the brightness of the radiation source is proportional to the average radiation power and is inversely proportional

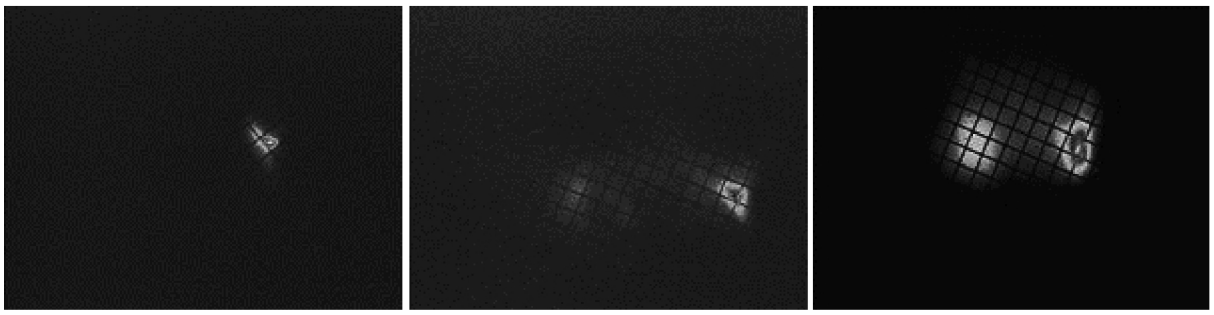

a b c

Figure 6. Images of plasma emitting in the EUV range at the parameters of the initiating laser $P = 1.6\times10^9$ (a) and 10^8 W cm^{-2} (b), and the sum of 20 images of initiating laser pulses at $P = 10^8$ W cm^{-2} and $f = 1$ kHz (c). The grid step is 0.4×0.4 mm.

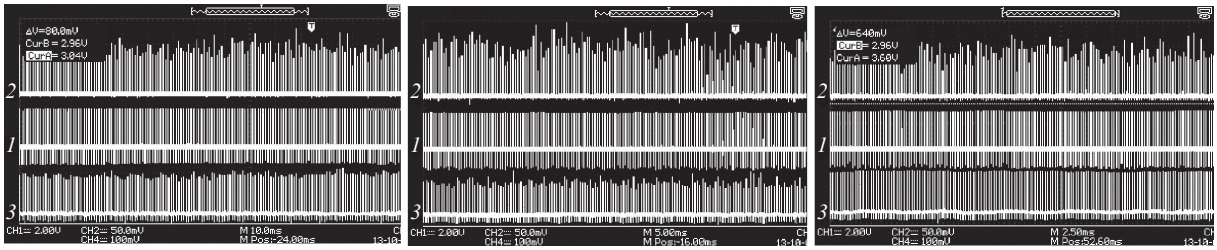

a b c

Figure 7. Series of voltage pulses (*1*), of EUV radiation (*2*) and of laser energy (*3*) at $f = 1$ (a), 2 (b) and 4 kHz (c).

to the area of emitting plasma, from the above discussion it appears that for creating a high-brightness EUV source on the basis of laser-induced plasma it is necessary to employ the laser with a power density of at least 10^9 W cm^{-2}. In addition, small values of etendue cannot be obtained at large areas of emitting plasma.

3.2. Repetitively pulsed regime of source operation

Sequences of voltage pulses, EUV radiation and laser energy, obtained at various pulse repetition rates and at a constant energy deposition of 3 J into the discharge are shown in Fig. 7. In these experiments, the laser with $P = 2.3\times10^8$ W cm^{-2} and the cathode tin jet with a cross section of 10×0.3 mm were used. Note that due to constructive features of this initiating laser, at $f \geqslant 4$ kHz its generation energy was rather greater and the pulse stability was better than at lower pulse repetition rates. In Fig. 7 one can see that the level of the EUV signal and, consequently, CE are almost constant up to at least $f = 4$ kHz; however, one should take into account that at higher rates the velocity of tin jets should also be increased: at $f = 1$ kHz the velocity of the tin jet was 3.5 m s^{-1}; at $f = 2$ kHz it was 6 m s^{-1} and at $f = 4$ kHz it was 8 m s^{-1}. Thus, with this kind of the EUV source and with the laser, possessing $P \approx 10^9$ W cm^{-2} and pulse repetition rate of above 4 kHz, by employing a more powerful high-voltage rectifier, one may expect to reach the radiance of at least 200 W (mm^2 sr)$^{-1}$ in the range $\lambda = 13.5\pm0.135$ nm.

One more important parameter of high-brightness EUV sources applicable to mask inspection in diagnostic complexes is the stability of the EUV signal from pulse to pulse. The relative standard deviations for the pulse sequences shown in Fig. 7 are σ = (a) 13%, (b) 21% and (c) 18%; this, of cause, is not sufficient for a diagnostic EUV source. Investigations conducted show that the pulse-to-pulse stability of the EUV signal in our source is mainly determined by the state of the tin surface in the domain where the radiation of the initiating laser is focused. It is known that laser plasma mainly spreads in a normal direction to the surface onto which the laser radiation is focused. Hence, even small deviations of the tin surface from a plane shape within the limits of the focused beam spot affect both the directions of the plasma spread and the plasma concentration, which results in different conditions of formation for the discharge current. This inevitably changes the energy characteristics of EUV radiation. Tin jet images obtained with a high-speed camera confirm this speculation. Figure 8 presents a negative photo of the tin jet of size 10×0.3 mm having the velocity of 9 m s^{-1}, flashed by a scattered radiation of a Nd:YAG laser. Dark structures on the

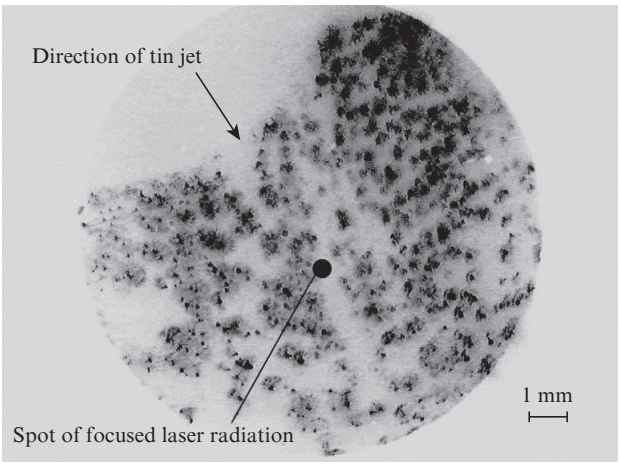

Figure 8. Photo (negative) of the tin jet with a cross section 10×0.3 mm flashed by a Nd:YAG laser ($v = 9$ m s^{-1}).

photo are the areas that strongly reflect laser radiation; these structures correspond to a convex relief on the jet surface. A focused laser spot and the direction of the tin jet are also marked in Fig. 8. One can see that the characteristic dimensions of irregularities on the surface of the plane jet are within the range of 0.1–1 mm, and the diameter of the focused laser spot (approximately 0.5 mm) also fits this range. Most probably, in the conditions of a turbulent flow (Re ≈ 1300–3800), the irregularities observed on the jet surface are related with generation of turbulent micro-vortices, the size and shapes of which depend on various factors: the roughness of channel walls and exit blade, profile of output hole, wettability of nozzle material by liquid tin, size and shape of the jet cross section, etc. Keeping in mind the nonstationary character of arising irregularities and, hence, of laser radiation focused to these areas, one can understand the nature of the unstable EUV signal. At low jet velocities (3–4 m s^{-1}), a fewer number of irregularities were observed on the surface. At a higher jet velocity, the number of irregularities increased, which confirms the results of signal stability measurements presented in Fig. 7. From the jet configurations tested, the best results from the viewpoint of the EUV signal stability were obtained with the cathode jet having the cross section of 10×0.3 mm. However, the configuration of the anode jet is not so critical with respect to the EUV signal stability. Hence, for enhancing the stability of the EUV signal, further investigations of this kind of the EUV source should be aimed at finding the conditions of forming tin jets with a minimal number of irregularities on their surfaces.

A dependence of the value of the EUV signal on the jet velocity has been studied. The experiments have been performed at f = 4 kHz. Pulse sequences of EUV signals were recorded at various jet velocities. An average energy of EUV radiation pulses and the corresponding standard deviation versus the tin jet velocity are presented in Fig. 9. One can see that an increase in the average energy of the EUV signal was only observed at velocities of up to v = 6 m s^{-1}, whereupon the energy was almost constant. At v = 6 m s^{-1} and f = 4 kHz, the corresponding distance S between neighbouring focusing spots of laser radiation on a jet surface will be 1.5 mm. Lest the focusing spots from successive laser pulses should overlap, the condition $S/d \geqslant 3$ (d is the diameter of a focal spot) should be satisfied. By extrapolating the results obtained to pulse repetition rates above 4 kHz, one may conclude that at f = 8 kHz the required jet velocity is at least 12 m s^{-1}, and at f = 16 kHz it is 24 m s^{-1}. Such jet velocities correspond to the pump output pressures of 5.2 and 21 atm, respectively.

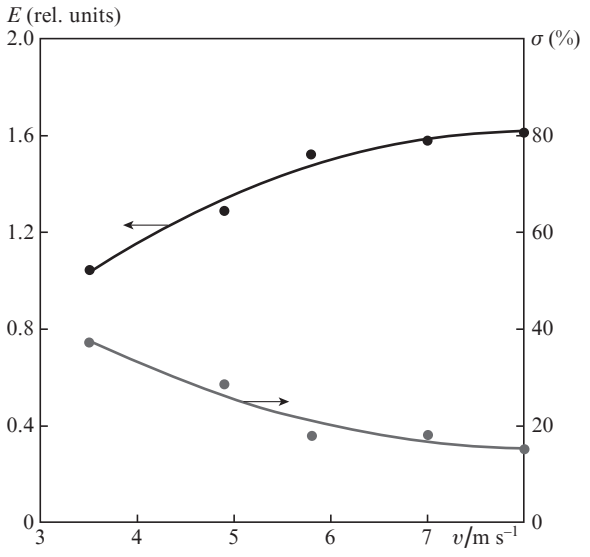

Figure 9. Dependence of the average energy of EUV radiation pulses and its standard deviation on the tin jet velocity (f = 4 kHz).

3.3. Spectrum of tin plasma

Figure 10 shows the spectrum of tin plasma emitting in the EUV range that was obtained by using a laser with P = 1.6×10^9 W cm^{-2}. Also, the working range of projection EUV lithography (λ = 13.5±0.135 nm) is marked along with the correspondence of various peaks to various tin ion states. One can see that tin ions from Sn^{8+} to Sn^{13+} contribute into the emission in the range mentioned. From the spectrum in Fig. 10 one may estimate the ratio of the energy emitted in the range λ = 13.5±0.135 nm to the energy emitted over the whole EUV range (in our case this ratio is 1/9).

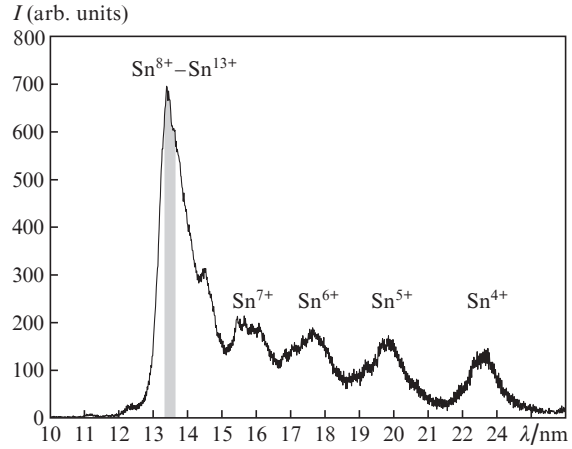

Figure 10. Spectrum of tin plasma of the EUV source.

4. Conclusions

The result of the work presented is the creation of a new kind of laser-induced electro-discharge sources on the basis of tin plasma emitting in the EUV range at a wavelength of $\lambda \approx$ 13.5 nm. The specific feature differing this source from other types of electro-discharge laser-induced plasma sources is an actually unlimited service life of the electrodes, which are realised as liquid tin jets circulating through a closed loop under the action of a specially designed centrifugal pump. The discharge in the EUV source has been initiated by the radiation of a Nd:YAG laser focused to one of the jets. A low-inductance pulsed circuit feeding the discharge is synchronised with the pulses of the initiating laser. The technologies developed and investigated while constructing the source, can be used in various applications of projection EUV lithography, in particular, in creating EUV sources for diagnostic complexes intended for mask inspection. With the initiating laser possessing the power density of about 10^9 W cm^{-2} the obtained efficiency of conversion to EUV radiation is approximately 2%/2π sr, and the size of the emitting plasma domain is about 0.2×0.35 mm. It has been demonstrated that the energy

parameters of EUV radiation remain constant up to a pulse repetition rate of at least 4 kHz. It has been shown that in the range $\lambda = 13.5 \pm 0.135$ nm the brightness of the EUV source created may reach 200 W $(mm^2\ sr)^{-1}$ and more. The physical factors determining the stability of the EUV radiation energy from pulse to pulse have been revealed, and the method for improving the radiation stability at high pulse repetition rates has been developed.

A centrifugal pump has been created for pumping melted tin, which provides the tin jet velocities of up to 15 m s^{-1}. A reliable pulsed scheme for discharge initiation has been developed with the energy deposited into the discharge of up to 4 J and the maximal pulse repetition rate of 8 kHz.

Acknowledgements. The work was supported by the RF Ministry of Science and Education [Agreement No. 14.579.21.0004, unique identifier of applied scientific research (project) RFMEFI57914X0004].

References

1. Bakshi V. (Ed.) *EUV source for Lithography* (Bellingham, Wash.: SPIE Press, 2006).
2. Attwood D. *Soft X-Rays and Extreme Ultraviolet Radiation* (Cambridge: Cambridge University Press, 2007).
3. Banine V.Y., Koshelev K.N., Swinkels G.H.P.M. *J. Phys. D: Appl. Phys.,* **44**, 253001 (2011).
4. Borisov V.M., Borisova G.N., Vinokhodov A.Yu., Zakharov S.V., Ivanov A.S., Kiryukhin Yu.B., Mishchenko V.A., Prokof'ev A.V., Khristoforov O.B. *Kvantovaya Elektron.*, **40**, 720 (2010) [*Quantum Electron*., **40**, 720 (2010)].
5. Brandt D.C., Fomenkov I.V., Farrar N.R., La Fontaine B., Myers D.W., Brown D.J., Ershov A.I., Sandstrom R.L., Vaschenko G.O., Böwering N.R., Das P., Fleurov V., Zhang K., Srivastava S.N., Ahmad I., Rajyaguru C., De Dea S., Dunstan W.J., Baumgart P., Ishihara T., Simmons R., Jacques R., Bergstedt R., Wittak C., Rafac R., Grava J., Schafgans A., Tao Y., Hoffman K., Ishikawa T., Evans D., Rich S., Boumen R., Meiling H., Peeters R., Kazinczi R., Harned N. *Int. EUVL Symp.* (Toyama, Japan, 2013).
6. Tchikoulaeva A., Miyai H., Suzuki T., Takehisa K., Kusunose H., Yamane T., Terasawa T., Watanabe H., Inoue S., Mori I.J. *Micro/Nanolithogr. MEMS MOEMS*, **13** (2), 023010-1-9 (2014).
7. Seidel P. *Int. EUVL Symp.* (Sapporo, Japan, 2007).
8. Rollinger B., Gambino N., Giovannini A.Z., Bozinova L.S., Alickaj F., Hertig K., Abhari R.S. *Proc. SPIE Int. Soc Opt. Eng.*, **9048**, 90482K1-9 (2014).
9. Teramoto Y., Santos B., Mertens G., Kops R., Kops M., Küpper F., Niimi G., Yabuta H., Nagano A., Yokoyama T., Yoshioka M., Shirai T. *Proc. SPIE Int. Soc Opt. Eng.,* **9048**, 904813-1-8 (2014).
10. Partlow M.J., Besen M.M., Blackborow P.A., Collins R., Gustafson D., Horne S.F., Smith D.K. *J. Micro/Nanolithogr. MEMS MOEMS*, **11** (2), 021105 (2012).
11. Koshelev K., Krivtsun V., Ivanov V., Yakushev O., Chekmarev A., Koloshnikov V., Snegirev E., Medvedev V. *J. Micro/Nanolithogr. MEMS MOEMS*, **11** (2), 021103-1-6 (2012).
12. Yakushev O.F.,Vinokhodov A.Yu., Koshelev K.N., Krivtsun V.N. *Instrum. Exp. Tech.*, **58** (6), 820 (2015).